COMMUNICATIONS CHEMISTRY

ARTICLE

DOI: 10.1038/s42004-018-0090-3 OPEN

A tunable lanthanide cubane platform incorporating air-stable radical ligands for enhanced magnetic communication

Gabriel Brunet[1], Milad Hamwi[1], Maykon A. Lemes[1], Bulat Gabidullin[1] & Muralee Murugesu[1]

The unique properties of polynuclear cluster-aggregates have long been staples in the molecular magnetism community. The initial success observed in high nuclearity transition metal complexes for generating exciting magnetic behaviors however, has not yet fully been extended to lanthanide-based clusters. This is in part due to the challenges related to promoting non-negligible magnetic interactions between two lanthanide ions. One promising route towards improving magnetic communication involves the incorporation of radical species. Here, we describe the preparation of tetranuclear $[Dy_4(\mu_3\text{-}OH)_4]^{8+}$ core structures that allow the incorporation of air-stable radical ligands. This combination paves the way for magnetically relevant lanthanide cubane cluster-aggregates capable of strong magnetic communication and improved spin-reversal barriers. Moreover, we show that the addition of electron donating groups lead to non-negligible antiferromagnetic coupling between the Dy^{III} centers and the $BPyTz^{\bullet -}$ ligands, while also simultaneously improving the slow magnetic relaxation dynamics in the absence of an applied field.

[1] Department of Chemistry and Biomolecular Sciences, University of Ottawa, Ottawa, ON K1N 6N5, Canada. Correspondence and requests for materials should be addressed to M.M. (email: m.murugesu@uottawa.ca)

The field of molecular magnetism saw a major breakthrough following the remarkable discovery that a nanosized $\{Mn_{12}\}$ cluster-aggregate could exhibit a bistable magnetic ground state and magnetic hysteresis[1]. This seminal work laid the foundation for decades worth of research into improving and perfecting control over the magnetic relaxation times of single-molecule magnets (SMMs)[2,3]. In fact, up until recently, high-nuclearity cluster-aggregates based on first row transition metal ions were leading candidates in the design of data storage devices and quantum information processors[4–6]. This is in part due to the fact that such large cluster-aggregates have proven to be uniquely tunable, where chemical modifications on the capping ligands can be readily introduced. Such modifications, while seemingly trivial, can lead to a drastic alteration in the magnetic behavior through, for example, a reorientation of the magnetic anisotropy axes[7–9]. Thus, multiple synthetic strategies have been devised over the years in order to fine-tune and promote certain magnetic features in high-nuclearity cluster-aggregates of first row transition metal ions[10,11]. Despite this, progress toward improving the two defining SMM characteristics, energy barrier (U_{eff}) and blocking temperature (T_B), remained slow.

The recent shift towards *4f* ions in the field of molecular magnetism, however, has yielded impressive growth in mononuclear and dinuclear SMMs; largely due to the inherent magnetic anisotropy of the lanthanide elements[12–15]. Recently, our research efforts in the development of dinuclear SMMs stem from a desire to understand and overcome the challenges related to the magnetic coupling of core *4f* orbitals[16,17]. Due to the lack of strong magnetic coupling, the enhancement and control of the magnetic properties of lanthanide cluster-aggregates remain relatively lackluster. For example, progress thus far in the SMM behavior of lanthanide cubane structures, which mimics a plethora of mixed-valent cubane Mn^{III}/Mn^{IV} complexes, has largely focused on the level of distortion within the $[Ln_4(\mu_3\text{-}OH)_4]^{8+}$ core[18–20]. It has previously been shown that larger Ln-OH-Ln angles can lead to a marginal improvement of their SMM-like properties; however in part due to the lack of significant magnetic coupling between the lanthanide ions, new strategies must be brought forward in order to further enhance their appeal and performance. In fact, they behave like a collection of single-ion magnets rather than a magnetically coupled system. If coupling could be introduced, however, akin to high-nuclearity transition metal complexes, lanthanide cluster-aggregates may also potentially lead to high performing exchange-coupled SMMs. Here, we propose an avenue to reinvigorate the field of magnetic lanthanide cubane cluster-aggregates, by incorporating air-stable radical ligands within their frameworks, thereby promoting non-negligible magnetic interactions. This work focuses on the non-innocent redox properties of 3,6-bis(3,5-dimethylpyrazol-1-yl)−1,2,4,5-tetrazine (BPyTz), whose coordination to first row transition metal ions has previously yielded anionic air-stable radicals ($BPyTz^{\bullet-}$)[21,22]. The ability of this ligand to generate air-stable radicals is rather unique compared to other radical-bridged systems, such as those based on 2,2′-bipyrimidine[23], N_2[24], or tetrapyridophenazine[25], all of which are highly unstable in air and require strong reducing agents during synthesis. In the compounds presented herein, we observe the spontaneous generation of a radical upon metal coordination, and under ambient conditions. Moreover, we have yet to encounter any 1,2,4,5-tetrazine-ring opening reactivity in BPyTz, which has been observed in a closely related 3,6-bis(2′-pyrimidyl)−1,2,4,5-tetrazine (BPymTz) organic ligand[26]. These features render the open-shell $BPyTz^{\bullet-}$ ligand an ideal building block with which to facilitate and promote direct exchange coupling with lanthanide ions, despite deeply buried *4f* orbitals.

With this in mind, we demonstrate that the judicious combination of ligand frameworks can lead not only to highly complex structures, but can also allow for the targeted enhancement of specific magnetic properties. Thus, we present our investigations into precisely constructed radical-bearing $[Dy^{III}_4]$ cubane cluster-aggregates, and their capacity to induce strong magnetic communication and zero-field SMM behavior, features that have seldom been achieved in Ln^{III}-based cluster-aggregates. The incorporation of three distinct organic linkers within a single molecular system, affords a level of control that can be exploited to rationally fine-tune the properties of the cubane structure. As a proof of concept, we are able to tune the electronics of a single ligand while maintaining an identical structural core, and subsequently observe the impact on the magnetic behavior. We first elect to combine the organic building block BPyTz with acetate- and β-diketonate-based anions (Fig. 1), therefore allowing us to tune the electronics of the overall cluster-aggregate through the addition of electron withdrawing and/or donating groups. The implementation of such a strategy, which relies on modifying the functionalization of peripheral ligands, has become one of the most predominant methods for enhancing the slow magnetic relaxation properties of Ln^{III} SMMs[17,27–30]. This is in part due to the ease at which such modifications can be characterized in the solid-state, and the drastic improvements in the energy barriers that have been experimentally observed thus far. Our investigations into this radical-bridged $[Dy^{III}_4]$ cubane lead us to two promising variants that significantly outperform a closely related structure[31]. By adding strongly electron withdrawing fluorine groups on the OAc^- moiety and using either $acac^-$ (acetylacetonate) or DBM^- (dibenzoylmethanide), we are able to not only change the direction of the magnetic anisotropy axis, leading to improved SMM behavior, but also examine the effect of imparting a slightly electron donating group on the $acac^-$ molecules by the addition of phenyl moieties. The resulting complexes are formulated as $[Dy_4(\mu_3\text{-}OH)_4(BPyTz^{\bullet-})_2(TFA)_2(a\text{-}cac)_4)]$ (**1**) and $[Dy_4(\mu_3\text{-}OH)_4(BPyTz^{\bullet-})_2(TFA)_2(DBM)_4)]\cdot 4(C_7H_8)$ (**2**), where TFA corresponds to trifluoroacetate. As such, we report the synthetic and structural details of radical-bridged lanthanide cubane cluster-aggregates, accompanied by an analysis of their magnetic behavior.

Results

Synthesis and structure. The synthesis of the desired cubane cluster-aggregate is promoted by the preparation of the Dy^{III} salt containing the selected terminal ligand (i.e. $Dy(DBM)_3$ and $Dy(TFA)_3$). The combination of two such precursors with BPyTz in a mixture of dichloromethane and tetrahydrofuran yields the cubane architecture (Fig. 1). It should be noted that the presence of hydroxide anions in the $[Dy_4(\mu_3\text{-}OH)_4]^{8+}$ core, despite the lack of a clear source of OH^-, is likely due to the use of hydrated metal salts and/or non-dried solvents. This has commonly been observed in the benchtop chemistry of large polynuclear transition metal- and lanthanide-based complexes[32,33]. The formation of a radical species under aerobic conditions can be readily distinguished in solution by the formation of either dark green or purple solutions. Crystallization of **1** and **2** is achieved by the slow vapor diffusion of an anti-solvent into the reaction medium. Full crystallographic data are provided in Supplementary Table 1 and Supplementary Methods. The two cluster-aggregates crystallize in the monoclinic *C*2/*c* space group and share the same $[Dy_4(\mu_3\text{-}OH)_4]^{8+}$ core. The external coordination environment is completed by two $BPyTz^{\bullet-}$ radical ligands, two bidentate TFA^- anions, and four $acac^-$ (**1**) or four DBM^- (**2**) molecules (Fig. 1). Evidence for the in-situ one electron reduction of the BPyTz ligand is first provided by investigating the N-N bond lengths within the tetrazine moiety. Indeed, elongation of this bond beyond 1.36 Å would suggest the formation of a tetrazine-based radical anion, which is anticipated to lead to strong

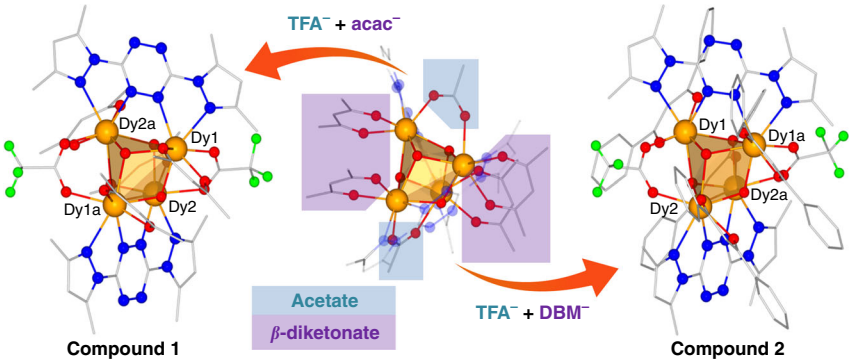

Fig. 1 General synthetic route to isolate the described lanthanide-based cubane structures. The molecular structures of **1** and **2** are displayed, and highlight the tunability of the selected $[Dy_4(\mu_3\text{-}OH)_4]^{8+}$ core. The combination of BPyTz with acetate- and β-diketonate-based ligands allows the facile modulation of their magnetic properties. Orange, red, blue, and green spheres represent Dy, O, N, and F atoms, respectively, while gray vertices represent C atoms. Solvent molecules, disordered components, and H atoms are omitted for clarity

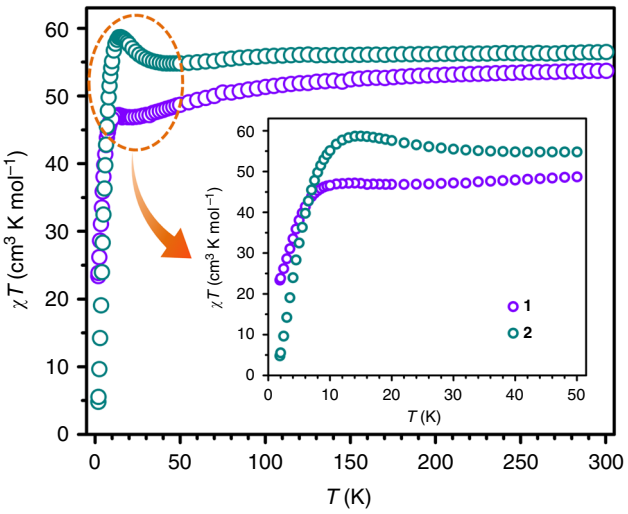

Fig. 2 Temperature dependence of the χT product at 1000 Oe for **1** and **2**. The inset displays a zoomed-in region of the same plot at low temperatures

magnetic exchange[34–37]. Here, the average N-N bond lengths within the tetrazine moiety correspond to 1.38 and 1.39 Å, respectively, for **1** and **2**, a clear indication of the reduced nature of the tetrazine-based ligand. The two crystallographically independent Dy^{III} ions are 8-coordinate and are best described by a square antiprismatic geometry—at the exception of Dy1 in **1**, which most closely resembles a biaugmented trigonalprism—as indicated by the SHAPE software (Supplementary Table 2)[38]. The heavily distorted nature of the cubane core is highlighted by average Dy-OH-Dy angles of 106.33 and 106.44° for **1** and **2**, respectively. It is also noteworthy that the unit cells of both complexes contain only four instances of the radical-bridged Dy^{III} cluster-aggregate, a vast improvement over the 18 molecules found in the unit cell of a related compound investigated by ab initio calculations[28]. This also serves to significantly simplify crystal-packing effects that could potentially be observed in the bulk magnetic properties. Moreover, in the structure of **2**, four partially disordered toluene molecules have been identified in the lattice. The closest intercluster Dy-Dy distances are 10.88 and 11.25 Å for **1** and **2**, respectively. Other relevant bond distances can be found in Supplementary Table 3.

DC magnetic susceptibility. To probe potentially exciting magnetic properties arising from the introduction of a radical ligand within the cubane cluster-aggregate, we first performed static direct current (dc) magnetic susceptibility measurements between 1.8 and 300 K under an applied field of 1000 Oe (Fig. 2). The observed room temperature values of 53.71 and 56.49 cm^3 K mol^{-1} for **1** and **2**, respectively, are in close agreement with the 57.43 cm^3 K mol^{-1} expected for four Dy^{III} centers and two $BPyTz^{\bullet-}$ radical anions ($g = 2.0$). In both complexes, the χT product remains relatively constant until ~75 K, where we observe a slight decrease followed by an increase that is more pronounced in **2**. The maximum χT values are 47.16 and 58.69 cm^3 K mol^{-1} at 14 and 15 K, respectively for **1** and **2**. The initial decrease at higher temperatures (25–100 K) is likely attributed to the thermal depopulation of Stark sublevels, while the distinct increase at low temperatures (~8–30 K) is due to the spin alignment of the metal centers caused by non-negligible antiferromagnetic interactions between the Dy^{III} ions and the $BPyTz^{\bullet-}$ radicals[39–42]. In addition to this, the fact that the increase is much more drastic in **2** compared to **1**, and occurs at a higher temperature, can be rationalized by a more significant coupling between the Dy^{III} metal centers and the ligand radical. This is further evidenced by the shorter Dy-N distances in **2** between the Dy^{III} ions and the nitrogen atoms originating from the tetrazine ring (2.47 Å in **1** versus 2.45 Å in **2**). This enhancement in the magnetic coupling strength, brought upon by the simple replacement of $acac^-$ with DBM^- ligands, exemplifies the impact of electron-donating groups on the resulting magnetic interactions. Here, the addition of phenyl groups serve to simultaneously reduce the average Dy-O distance of the β-diketonates from 2.34 Å in **1**, to 2.30 Å in **2**, while also shortening the aforementioned Dy^{III}-radical distances (Supplementary Figure 2). The final decrease in the χT (below 10 K) can be attributed to intermolecular antiferromagnetic interactions, as reported in a molecular analog[31]. The strength of the intramolecular interactions in **2** can further be observed in the corresponding M versus H plot which displays a distinctive "S-shape" curve, while no such feature exists in **1** (Supplementary Figure 1).

AC magnetic susceptibility. In order to verify the possibility of single-molecule magnet behavior, we performed alternating current (ac) magnetic susceptibility measurements on **1** and **2**. In both cases, we observe an ac signal under 0 Oe dc field; however, in the case of **1**, only tails of peaks are observed within the limits of the magnetometer (Fig. 3). The shifting of the peaks in the out-of-phase (χ'') magnetic susceptibility as a function of frequency are indicative of slow magnetic relaxation. Interestingly, the intensity of the peaks diminishes with decreasing temperatures.

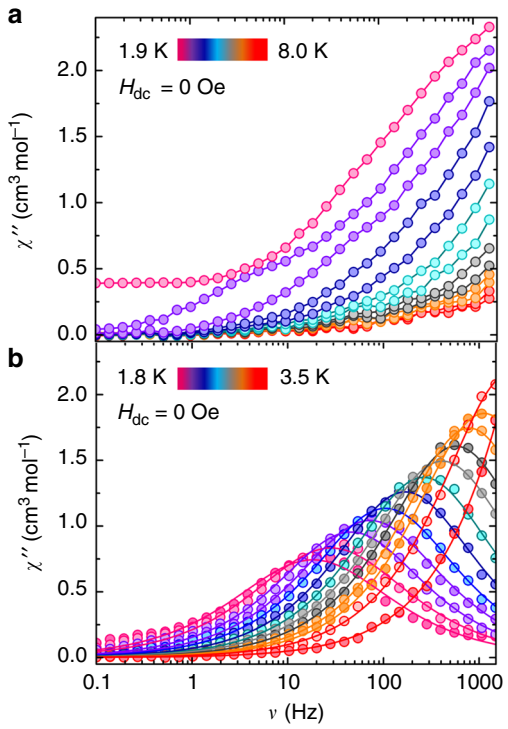

Fig. 3 Slow magnetic relaxation observed by SQUID magnetometry. Frequency dependence of the out-of-phase (χ'') magnetic susceptibility under 0 Oe dc field for **1** (**a**) and **2** (**b**). For **1**, the solid lines serve as guides for the eyes while in **2**, they represent the best fit to a generalized Debye model

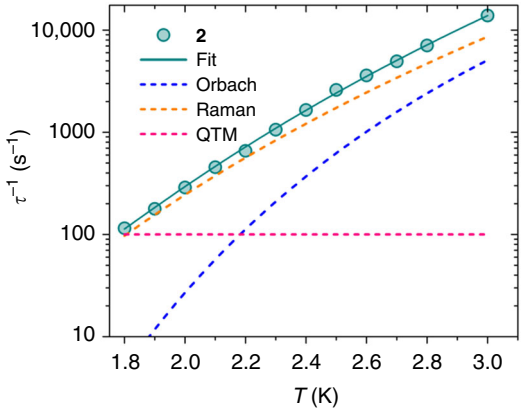

Fig. 4 Temperature dependence of the magnetic relaxation times. The solid line represents the best-fit taking into account contributions from Orbach, Raman and QTM. The dashed lines indicate the individual contributions of each relaxation mechanism

This is in sharp contrast to the vast majority of SMMs, where the inverse behavior is observed; a decrease in the temperature is generally accompanied by an increase in the χ'' intensity[43,44]. Such a feature further confirms the strength of the antiferromagnetic interactions between the Dy^{III} ions and the $BPyTz^{\bullet -}$ radical, and is reflective of the drastic decrease of χ at low temperatures. Fitting of these data using a generalized Debye equation yields the magnetic relaxation times (τ) for **2** in the temperature range of 1.8–3.5 K. In turn, the dominant magnetic relaxation mechanisms responsible for spin reversal can be evaluated by an analysis of the temperature dependence of the relaxation times (Fig. 4). In order to reproduce the temperature dependence of the relaxation time, we have fit τ^{-1} versus T taking into account Orbach, Raman and quantum tunneling of the magnetization (QTM) processes, as given in Eq. (1). The direct process was omitted here due to the fact that the ac measurements were performed under zero dc field.

$$\tau^{-1} = \tau_0^{-1} \exp\left[-U_{\mathrm{eff}}/(k_{\mathrm{B}}T)\right] + CT^n + \tau_{\mathrm{QTM}}^{-1} \qquad (1)$$

The resulting fit is in good agreement with all data and afforded $\tau_0 = 5.51(9) \times 10^{-9}$ s, $U_{\mathrm{eff}}/k_{\mathrm{B}} = 31.44(3)$ K, $C = 0.55(5)$ s^{-1} K$^{-8.78}$, $n = 8.7(8)$ and $\tau_{\mathrm{QTM}} = 8.44(8) \times 10^{-3}$ s. Notably, the Raman exponent (n) is close to the expected value of $n = 9$ for a Kramers systems. The attempt time (τ_0) is also well within the expected range for single-molecule magnets (10^{-6} to 10^{-10} s). Moreover, the spin-reversal barrier (U_{eff}) is in line with the one approximated using an Arrhenius plot (36.53(5) K; Supplementary Figure 3). This value represents the third highest energy barrier at zero field within the class of Ln_4 cubanes (Supplementary Table 4)[45–47]. Thus, we demonstrate that the incorporation of open-shell ligands can improve the magnetic performance of Ln^{III}-based cluster-aggregates, however, at the same time, we maintain that such a feature cannot exclusively be relied on in order to optimize the anisotropy barrier. Additional factors such as dipolar exchange interactions and the symmetry of the Ln^{III} ions are also expected to play decisive roles.

Direction of the magnetic anisotropy. Since the ground state of **1** and **2** is defined by $m_J = \pm 15/2$, it is amenable to electrostatic analysis by Magellan[48], providing an estimation of the orientation of the magnetic anisotropy axes (Fig. 5). Here, we find that the main magnetic axes are oriented towards either the TFA^- anions or the center of the tetrazine ring. The two distinct orientations are a by-product of having two crystallographically independent Dy^{III} ions within each cubane. It is interesting to note that the anisotropy axes in **2** are well aligned with the ideal axes generated from the Dy^{III} centers to the two aforementioned ligands. In fact, the deviation in **2** from TFA^- is only 5.19°, while the one from the tetrazine ring is calculated to be 12.2°. This is in contrast to **1**, where the deviation is more significant, with analogous angles calculated to be 21.8° and 17.8°, respectively. The implication of this result is that the chemical modification of secondary ligands ($acac^-$ versus DBM^-) can influence the orientation of the magnetic anisotropy axis. The greater electron-donating ability of DBM^- compared to $acac^-$ yields stronger interactions with the $BPyTz^{\bullet -}$ radical, which in turn may shift the magnetic anisotropy axes toward the more negatively charged species so as to achieve greater minimization of the electrostatic potential energy.

Discussion

In summary, we report the incorporation of air-stable radicals within lanthanide cubane cluster-aggregates. Modulation of the capping ligands has allowed for a significant improvement of the magnetic behavior in terms of both magnetic coupling strength and relaxation barrier. This is in contrast to other lanthanide cubane structures that are generally obtained serendipitously and lack any real tunability of their physical properties. Using an identical $[Dy_4(\mu_3\text{-}OH)_4]^{8+}$ core structure, we have improved the out-of-phase magnetic susceptibility—from tails of peaks to frequency- and temperature-dependent ac signals—yielding an effective spin reversal barrier of 31 K in the absence of an applied field. Thus, we provide a blueprint towards improving the single-molecule magnet behavior of lanthanide-based cluster-aggregates. Further adjustments to the ligand field from the capping ligands could promote even stronger magnetic interactions between the lanthanide ions and lead to desired remanent magnetization.

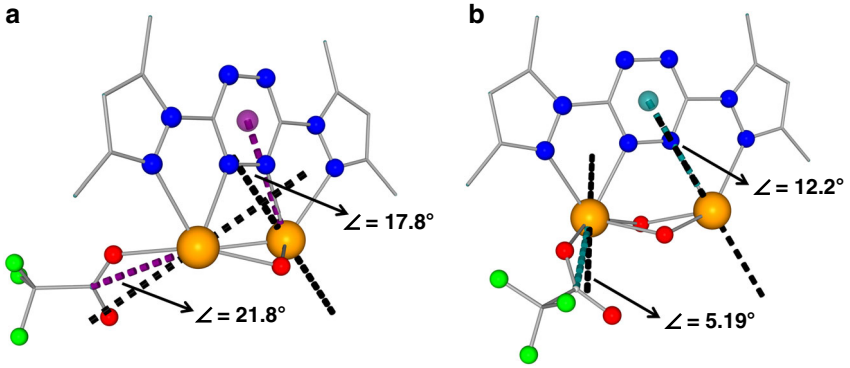

Fig. 5 Magnetic axes. Electrostatic orientation of the main magnetic axes for the ground doublet of the two crystallographically independent Dy^{III} ions in **1** (**a**) and **2** (**b**), shown as dashed black lines. The dashed colored lines display the ideal orientation toward either the TFA^- anion or the centroid of the tetrazine ring, along with their respective angular deviations from the predicted anisotropy axis

Methods

Materials. The BPyTz ligand was prepared in accordance with previously reported methods[49], as was the metal salt $Dy(TFA)_3$[50]. The $Dy(DBM)_3$ starting material was synthesized following a previously published procedure but with slight modifications[51]. A solution of $DyCl_3{\cdot}6H_2O$ in water was added dropwise to an equimolar solution of DBM and piperidine in ethanol, under constant stirring. The molar ratio of Dy/DBM was 1:3. The precipitate was then washed with ethanol and air-dried.

Magnetic measurements. Magnetic susceptibility measurements were performed using an MPMS-XL7 Quantum Design SQUID magnetometer. Direct current (dc) susceptibility measurements were performed at temperatures ranging from 1.9 to 300 K and performed on a crushed polycrystalline sample of 24.2 (**1**) and 17.3 mg (**2**), wrapped in a polyethylene membrane. Alternating current (ac) susceptibility measurements were performed under an oscillating ac field of 3.78 Oe and ac frequencies ranging from 0.1 to 1488 Hz. Magnetization vs. field measurements were performed at 100 K in order to check for the presence of ferromagnetic impurities, which were found to be absent. The magnetic data were corrected for diamagnetic contributions using Pascal's constants.

X-ray crystallography. The crystals of **1** and **2** were mounted on thin glass fibers using paraffin oil. Prior to data collection, the crystals were cooled to 200(2) K. The data were collected on a Bruker AXS single-crystal diffractometer equipped with a sealed Mo tube (wavelength 0.71073 Å) and APEX II CCD detector. Full refinement and collection details can be found in the Supplementary Methods and Supplementary Table 1

Preparation of $[Dy_4(\mu_3\text{-}OH)_4(BPyTz^{\bullet-})_2(TFA)_2(acac)_4]$ (1). $Dy(acac)_3{\cdot}xH_2O$ (0.25 mmol, 208.8 mg) and $Dy(TFA)_3$ (0.125 mmol, 62.7 mg) were dissolved in a solvent mixture of CH_2Cl_2/THF (1:1, 4 mL) and added to a 4 mL CH_2Cl_2 solution of BPyTz (0.125 mmol, 33.8 mg). The mixture was stirred for a few hours. The resulting dark purple solution was filtered under gravity. Dark green crystals were obtained by vapor diffusion using hexane as an antisolvent after approximately 2 days. Selected IR data for **1** (cm^{-1}): 3606(w), 1675(m), 1596(m), 1550(s), 1519(s), 1477(s), 1454(s), 1422(s), 1391(s), 1313(m), 1197(s), 1145(m), 1118(s), 1064(m), 1024(m), 983(m), 941(m), 841(m), 800(m), 784(m), 682(s). Elemental analysis: calcd for $Dy_4C_{51.5}H_{67}N_{16}O_{16}F_6$: C 28.39%; H 3.10%; N 10.29%. Found: C 28.86%; H 2.91%; N 10.31%. These results are consistent with ~3.5 CH_2Cl_2 solvent molecules contained within the lattice (see Supplementary Methods for details).

Preparation of $[Dy_4(\mu_3\text{-}OH)_4(BPyTz^{\bullet-})_2(TFA)_2(DBM)_4]{\cdot}4(C_7H_8)$ (2). $Dy(DBM)_3{\cdot}xH_2O$ (0.5 mmol, 229.9 mg) and $Dy(TFA)_3$ (0.25 mmol, 125.4 mg) were dissolved in a solvent mixture of CH_2Cl_2/THF (1:1, 5 mL) and added to a 5 mL CH_2Cl_2 solution of BpyTz (0.25 mmol, 67.6 mg). The mixture was stirred for a few hours. The resulting dark green solution was filtered under gravity. Black crystals were obtained by vapor diffusion using toluene as an antisolvent after ~2 days. Selected IR data for **2** (cm^{-1}): 3607(w), 2930(w), 2323(w), 1674(s), 1600(s), 1522(s), 1425(s), 1393(s), 1313(m), 1267(m), 1196(s), 1143(s), 1018(m), 984(m), 924(m), 842(m), 797(m), 699(s), 652(s), 616(m), 536(m). Elemental analysis: calcd for $Dy_4C_{116}H_{108}N_{16}O_{16}F_6$: C 50.73%; H 3.96%; N 8.16%. Found: C 50.07%; H 3.45%; N 7.79%.

Data availability

The X-ray crystallographic coordinates for the structures **1** and **2** are available as Supplementary Data 1 and 2, respectively. These data have also been deposited at the Cambridge Crystallographic Data Centre (CCDC), under deposition numbers CCDC1867341 (**1**) and CCDC1867342 (**2**). These data can be obtained free of charge from the CCDC via http://www.ccdc.cam.ac.uk/data_request/cif. The other data that support the findings of this study are available from the corresponding author upon reasonable request.

Received: 19 September 2018 Accepted: 1 November 2018
Published online: 28 November 2018

References

1. Sessoli, R., Gatteschi, D., Caneshi, A. & Novak, M. A. Magnetic bistability in a metal-ion cluster. *Nature* **365**, 141–143 (1993).
2. Tasiopoulous, A. J., Vinslava, A., Wernsdorfer, W., Abboud, K. A. & Christou, G. Giant single-molecule magnets: a $\{Mn_{84}\}$ torus and its supramolecular nanotubes. *Angew. Chem. Int. Ed.* **43**, 2117–2121 (2004).
3. Murrie, M., Teat, S. J., Stoeckli-Evans, H. & Güdel, H. U. Synthesis and characterization of a cobalt(II) single-molecule magnet. *Angew. Chem. Int. Ed.* **42**, 4653–4656 (2003).
4. Milios, C. J. et al. A record anisotropy barrier for a single-molecule magnet. *J. Am. Chem. Soc.* **129**, 2754–2755 (2007).
5. Barra, A. L. et al. Single-molecule magnet behavior of a tetranuclear iron(III) complex. The origin of slow magnetic relaxation in iron(III) clusters. *J. Am. Chem. Soc.* **121**, 5302–5310 (1999).
6. Yang, C.-I., Wernsdorfer, W., Lee, G.-H. & Tsai, H.-L. A pentanuclear manganese single-molecule magnet with a large anisotropy. *J. Am. Chem. Soc.* **129**, 456–457 (2007).
7. Zhu, Y.-Y. et al. A family of enantiopure Fe^{III}_4 single molecule magnets: fine tuning of energy barrier by remote substituent. *Dalton. Trans.* **43**, 11897–11907 (2014).
8. Cornia, A. et al. Energy-barrier enhancement by ligand substitution in tetrairon(III) single-molecule magnets. *Angew. Chem. Int. Ed.* **43**, 1136–1139 (2004).
9. Jones, L. F. et al. Tuning magnetic properties using targeted structural distortion: new additions to a family of Mn_6 single-molecule magnets. *Inorg. Chim. Acta* **361**, 3420–3426 (2008).
10. Waldmann, O. A criterion for the anisotropy barrier in single-molecule magnets. *Inorg. Chem.* **46**, 10035–10037 (2007).
11. Oshio, H., Hoshino, N. & Nakano, M. Single-molecule magnets of ferrous cubes: structurally controlled magnetic anisotropy. *J. Am. Chem. Soc.* **126**, 8805–8812 (2004).
12. Goodwin, C. A. P., Ortu, F., Reta, D., Chilton, N. F. & Mills, D. P. Molecular magnetic hysteresis at 60 kelvin in dysprosocenium. *Nature* **548**, 439–442 (2017).
13. Norel, L. et al. A terminal fluoride ligand generates axial magnetic anisotropy in dysprosium complexes. *Angew. Chem. Int. Ed.* **130**, 1951–1956 (2018).
14. Guo, F.-S. et al. A dysprosium metallocene single-molecule magnet functioning at the axial limit. *Angew. Chem. Int. Ed.* **56**, 11445–11449 (2017).
15. Demir, S., Gonzalez, M. I., Darago, L. E., Evans, W. J. & Long, J. R. Giant coercivity and high magnetic blocking temperatures for N_2^{3-} radical-bridged dilanthanide complexes upon ligand dissociation. *Nat. Commun.* **8**, 2144 (2017).
16. Long, J. et al. Single-molecule magnet behaviour for an antiferromagnetically superexchanged-coupled dinuclear dysprosium(III) complex. *J. Am. Chem. Soc.* **133**, 5319–5328 (2011).

17. Habib, F. et al. Significant enhancement of energy barriers in dinuclear dysprosium single-molecule magnets through electron-withdrawing effects. *J. Am. Chem. Soc.* **135**, 13242–13245 (2013).
18. Ke, H. et al. Magnetic properties of dysprosium cubanes dictated by the M-O-M angles of the $[Dy_4(\mu_3\text{-}OH)_4]$ core. *Inorg. Chem.* **49**, 7549–7557 (2010).
19. Miao, Y.-L. et al. Two novel Dy8 and Dy11 clusters with cubane $[Dy_4(\mu_3\text{-}OH)_4]^{8+}$ units exhibiting slow magnetic relaxation behaviour. *Dalton. Trans.* **40**, 10229–10236 (2011).
20. Yi, X., Bernot, K., Calvez, G., Daiguebonne, C. & Guillou, O. 3D organization of dysprosium cubanes. *Eur. J. Inorg. Chem.* **34**, 5879–5885 (2013).
21. Lemes, M. A. et al. Probing magnetic-exchange coupling in supramolecular squares based on reducible tetrazine-derived ligands. *Chem. Eur. J.* **24**, 4259–4263 (2018).
22. Tripathy, S. K. et al. A dinuclear $[\{(p\text{-}cym)Ru^{II}Cl\}_2(\mu\text{-}bpytz^{\bullet-})]^{+}$ complex bridged by a radical anion: synthesis, spectroelectrochemical, EPR and theoretical investigation (bpytz = 3, 6-bis(3,5-dimethyl-pyrazolyl)1,2,4,5-tetrazine; p-cym = p-cymeme). *Dalton. Trans.* **46**, 12532–12538 (2016).
23. Demir, S., Zadrozny, J. M., Nippe, M. & Long, J. R. Exchange coupling and magnetic blocking in bipyrimidyl radical-bridged dilanthanide complexes. *J. Am. Chem. Soc.* **134**, 18546–18549 (2012).
24. Rinehart, J. D., Fang, M., Evans, W. J. & Long, J. R. Strong exchange and magnetic blocking in N_2^{3-}-radical-bridged lanthanide complexes. *Nat. Chem.* **3**, 538–542 (2011).
25. Ma, X. et al. A redox-active bridging ligand to promote spin delocalization, high-spin complexes, and magnetic multi-switchability. *Angew. Chem. Int. Ed.* **57**, 7841–7845 (2018).
26. Lemes, M. A. et al. Study of a novel hepta-coordinated Fe^{III} bimetallic complex with an unusual 1,2,4,5-tetrazine-ring opening. *Polyhedron* **108**, 163–168 (2016).
27. Pedersen, K. S. et al. Modifying the properties of 4f single-ion magnets by peripheral ligand functionalisation. *Chem. Sci.* **5**, 1650–1660 (2014).
28. Langley, S. K. et al. Single-molecule magnetism in a family of $\{Co^{III}_2Dy^{III}_2\}$ butterfly complexes: effects of ligand replacement on the dynamics of magnetic relaxation. *Inorg. Chem.* **53**, 4303–4315 (2014).
29. Jiang, Y. et al. Terminal solvent effects on the anisotropy barriers of Dy2 systems. *Dalton. Trans.* **45**, 16709–16715 (2016).
30. Cucinotta, G. et al. Magnetic anisotropy in a dysprosium/DOTA single-molecule magnet: beyond simple magneto-structural correlations. *Angew. Chem.* **124**, 1638–1642 (2012).
31. Vieru, V. et al. Toward a microscopic understanding of the magnetization behavior of a multimolecular single crystal of radical-bridged $[Dy^{III}_4]$ cubane units: a joint ab initio, micro-superconducting quantum interference device, and electron paramagnetic resonance study. *J. Phys. Chem. C* **122**, 11128–11135 (2018).
32. Abbasi, P. et al. Transition metal single-molecule magnets: a {Mn31} nanosized cluster with a large energy barrier of ~60 K and magnetic hysteresis at ~5 K. *J. Am. Chem. Soc.* **139**, 15644–15647 (2017).
33. Lacelle, T., Brunet, G., Holmberg, R. J., Gabidullin, B. & Murugesu, M. Unprecedented octanuclear Dy^{III} cluster exhibiting single-molecule magnet behavior. *Cryst. Growth Des.* **17**, 5044–5048 (2017).
34. Lemes, M. A. et al. Strong ferromagnetic exchange coupling in a $\{Ni^{II}_4\}$ cluster mediated through an air-stable tetrazine-based radical anion. *Chem. Commun.* **53**, 8660–8663 (2017).
35. Dolinar, B. S. et al. Lanthanide triangles supported by radical bridging ligands. *J. Am. Chem. Soc.* **140**, 908–911 (2018).
36. Alexandropoulos, D. I., Dolinar, B. S., Vignesh, K. R. & Dunbar, K. R. Putting a new spin on supramolecular metallacycles: Co_3 triangle and Co_4 square bearing tetrazine-based radicals as bridges. *J. Am. Chem. Soc.* **139**, 11040–11043 (2017).
37. Woods, T. J. et al. Strong direct magnetic coupling in a dinuclear Co^{II} tetrazine radical single-molecule magnet. *Chem. Eur. J.* **21**, 10302–10305 (2015).
38. Casanova, D., Llunell, M., Alemany, P. & Alvarez, S. The rich stereochemistry of eight-vertex polyhedral: a continuous shape measures study. *Chem. Eur. J.* **11**, 1479–1494 (2005).
39. Zhang, P. et al. Exchange coupling and single molecule magnetism in redox-active tetraoxolene-bridged dilanthanide complexes. *Chem. Sci.* **9**, 1221–1230 (2018).
40. Rinehart, J. D., Fang, M., Evans, W. J. & Long, J. R. A N_2^{3-} radical-bridged terbium complex exhibiting magnetic hysteresis at 14 K. *J. Am. Chem. Soc.* **133**, 14236–14239 (2011).
41. Dolinar, B. S., Gómez-Coca, S., Alexandropoulos, D. I. & Dunbar, K. R. An air-stable radical-bridged dysprosium single molecule magnet and its neutral counterpart: redox switching of magnetic relaxation dynamics. *Chem. Commun.* **53**, 2283–2286 (2017).
42. Guo, F.-S. & Layfield, R. A. Strong direct exchange coupling and single-molecule magnetism in indigo-bridged lanthanide dimers. *Chem. Commun.* **53**, 3130–3133 (2017).
43. Guo, Y.-N. et al. Strong axiality and ising exchange interaction suppress zero-field tunneling of magnetization of an asymmetric Dy_2 single-molecule magnet. *J. Am. Chem. Soc.* **133**, 11948–11951 (2011).
44. Oyarzabal, I. et al. Rational electrostatic design of easy-axis magnetic anisotropy in a Zn^{II}-Dy^{III}-Zn^{II} single molecule magnet with a high energy barrier. *Chem. Eur. J.* **20**, 14262–14269 (2014).
45. Wong, H. Y., Chan, W. T. K. & Law, G.-L. Assembly of lanthanide(III) cubanes and dimers with single-molecule magnetism and photoluminescence. *Inorg. Chem.* **57**, 6893–6902 (2018).
46. Han, C.-B., Wang, Y.-L., Li, Y.-L., Liu, C.-M. & Liu, Q.-Y. Slow magnetization relaxation in a one-dimensional chiral dysprosium-carboxylate compound constructed from the cubic $Dy_4(\mu_3\text{-}OH)_4$ clusters. *Inorg. Chem. Commun.* **58**, 91–94 (2015).
47. Liu, C.-M., Zhang, D.-Q., Hao, X. & Zhu, D.-B. Syntheses, crystal structures, and magnetic properties of two p-tert-butylsulfonylcalix[4]arene supported cluster complexes with a totally disordered $Ln_4(OH)_4$ cubane core. *Cryst. Growth Des.* **12**, 2948–2954 (2012).
48. Chilton, N. F., Collison, D., McInnes, E. J. L., Winpenny, R. E. P. & Soncini, A. An electrostatic model for the determination of magnetic anisotropy in dysprosium complexes. *Nat. Commun.* **4**, 2551 (2013).
49. Coburn, M. D. et al. An improved synthesis of 3,6-diamino-1,2,4,5-tetrazine. II. *triaminoguanidine 2,4-Pent. J. Heterocycl. Chem.* **28**, 2049–2050 (1991).
50. Belyi, V. I., Rastorguev, A. A., Remova, A. A., Romanenko, G. V. & Sokolova, N. P. X-ray diffraction analysis and luminescent study of the structure of the $Tb_2(CF_3COO)_6(H_2O)_6$ dimer obtained from terbium(III) carbonate. *J. Struct. Chem.* **45**, 130–138 (2004).
51. Crosby, G. A. & Kasha, M. Intramolecular energy transfer in ytterbium organic chelates. *Spectrochim. Acta* **10**, 377–382 (1958).

Acknowledgements

We thank the Natural Sciences and Engineering Research Council of Canada (Discovery, DND Discovery Grant and Accelerator Supplements) for generous financial support and the University of Ottawa for essential infrastructure. G.B. gratefully acknowledges the support from NSERC (CGS-D).

Author contributions

M.H. and M.A.L. synthesized and characterized the materials. G.B. and M.M. measured and analyzed the magnetic properties. B.G. carried out the X-ray crystal structure refinement. G.B. and M.M. wrote and reviewed the manuscript.

Additional information

Supplementary information accompanies this paper at https://doi.org/10.1038/s42004-018-0090-3.

Competing interests: The authors declare no competing interests

Reprints and permission information is available online at http://npg.nature.com/reprintsandpermissions/

Publisher's note: Springer Nature remains neutral with regard to jurisdictional claims in published maps and institutional affiliations.